

# Monolayer Structure of Arachidic Acid on Graphite

Loji K. Thomas,<sup>†</sup> Angelika Kühnle,<sup>‡</sup> Sebastian Rode,<sup>‡</sup> Uwe Beginn,<sup>§</sup> and Michael Reichling<sup>\*,†</sup>

Fachbereich Physik, Universität Osnabrück, Barbarastrasse 7, 49076 Osnabrück, Germany, Institut für Physikalische Chemie, Johannes Gutenberg-Universität Mainz, Jakob-Welder-Weg 11, 55099 Mainz, Germany, and Institut für Chemie, Universität Osnabrück, Barbarastrasse 7, 49076 Osnabrück, Germany

Received: June 7, 2010; Revised Manuscript Received: August 31, 2010

The self-assembly of arachidic acid (C<sub>19</sub>H<sub>39</sub>COOH) at the liquid–solid interface between 1-phenyloctane (C<sub>6</sub>H<sub>5</sub>(CH<sub>2</sub>)<sub>7</sub>CH<sub>3</sub>) and highly oriented pyrolytic graphite (HOPG) is studied by scanning tunneling microscopy (STM) to identify the structure of the monomolecular film. We observe the formation of highly ordered domains with molecules oriented in three different orientations compatible with the symmetry of the HOPG substrate, a spontaneous enantiomeric separation of the pro-chiral molecules, and reveal structural details with submolecular resolution. To determine the surface unit cell with an intrinsic calibration to the substrate atomic structure, the intermolecular distance is precisely determined from the analysis of a STM image exhibiting a moiré pattern created by the superposition of current contributions from the molecular structure with contributions from the graphite atomic lattice. The dimensions of the unit cell accommodating two molecules are  $|a| = 0.94$  nm and  $|b| = 2.83$  nm with an angle of 85° between unit cell vectors **a** and **b**. The respective molecular arrangement allows hydrogen bonding between carboxylic groups with an unrelaxed O–O bond distance of 0.31 nm.

## 1. Introduction

Organic molecules are the conceptual, structural, and functional basis of numerous existing and envisaged nanotechnology applications, such as molecular light-emitting and -harvesting devices, molecular electronics, biological identification, and molecular sensor technologies. Because devices based on single molecules are still challenging for applications, systems involving molecular thin films appear to be the most promising for the near future.<sup>1,2</sup> Organic molecules are used due to their self-assembling ability; tunability of structural, chiral, electronic and chemical properties; and the many functions they can perform.<sup>3–5</sup> Self-assembly and the control of chiral properties on surfaces is one of the major routes toward novel molecular architectures<sup>6–13</sup> and is used, for instance, for the realization of electronic and optoelectronic devices.<sup>14–16</sup>

The visualization of molecular structures in real space at the atomic scale is most helpful for understanding the self-assembly process, and the liquid–solid interface is an excellent environment in which to probe them.<sup>17–19</sup> Organic molecules, though in general insulating, can be imaged with a scanning tunneling microscope (STM) when deposited on a conducting substrate such as graphite. Ever since the first unambiguous report of molecular adsorbates on graphite,<sup>20</sup> the STM has been widely used to study organic thin films on crystalline solid substrates.

Although not necessarily suitable for UHV conditions, graphite is a particularly favored substrate for STM studies at the liquid/solid interface. Major advantages of graphite compared with other electrically conducting surfaces are its chemical inertness and the ease of surface preparation. Although there is a fortuitous geometric similarity between the graphite surface structure and alkyl carbon zigzag chains (0.246 and 0.252 nm

bond lengths, respectively), the self-assembly of aliphatic chains on graphite<sup>21</sup> is not exclusively promoted by this feature because similar structures were also observed on other substrates that are atomically flat but without any geometric matching.<sup>22</sup> STM imaging at the liquid–graphite interface has given many insights into the structure and dynamics of these monolayers.<sup>23–30</sup> Most of the earlier work has been focused on the investigation of general trends of different species of molecules on the graphite surface and less on a detailed understanding of the monolayer structure.<sup>31</sup>

Here, we study the self-assembly of arachidic acid on highly oriented pyrolytic graphite (HOPG) by STM imaging. We chose this molecule because it is a well-known model system that has previously been studied in its basic structural details<sup>32,33</sup> and yields moiré contrast features in STM imaging that we use for an intrinsic calibration of STM images. The focus of our work is to yield submolecular resolution that allows us to investigate in detail the relative disposition of molecules and to precisely determine intermolecular distances. We are, for instance able to determine the O–O distance for arachidic acid dimers present on the surface, which has not previously been reported but is most important for completely evaluating the influence of the graphite substrate on the self-assembly process. We find a highly regular arrangement of flat lying molecules in stripes (lamellae) interconnected by the carboxylic functionalities of the arachidic acid molecules. From the STM measurements and their analysis as well as by exploiting moiré patterns formed by the molecular layer and the underlying substrate, we are able to derive accurate structural data of the molecular layer. Combining this with knowledge on the strength of interactions involved in the self-assembly, we can unambiguously identify one of several possible models as the structure of the arachidic monolayer on HOPG. This model yields an intermolecular distance of 0.47 nm and an unrelaxed O–O distance of 0.31 nm for the hydrogen bond between carboxylic dimers. It is an amendment of an earlier model proposing a smaller intermolecular distance.<sup>32</sup> An

\* To whom correspondence should be addressed. Phone: +49 541 969-2264. Fax: +49 541 969-12264. E-mail: reichling@uos.de.

<sup>†</sup> Fachbereich Physik, Universität Osnabrück.

<sup>‡</sup> Institut für Physikalische Chemie, Universität Mainz.

<sup>§</sup> Institut für Chemie, Universität Osnabrück.

analysis of larger scale STM images, furthermore, reveals the formation of molecular domains with directions compatible with the 3-fold symmetry of the HOPG substrate as well as a spontaneous separation of the pro-chiral molecules into enantiomeric pure domains.

## 2. Experimental Section

Arachidic acid ( $C_{19}H_{39}COOH$ ) as commercially available (99% pure, Acros Organics, Geel, Belgium) is dissolved in 1-phenyloctane (99% pure, Acros Organics) to obtain a nearly saturated solution. The solution is sonicated and kept at room temperature before applying it to a freshly cleaved sample of highly oriented pyrolytic graphite (HOPG) (ZYG grade, SPI Supplies, West Chester, PA, USA). STM images are taken in the constant current mode at ambient conditions with a compact commercial STM (Nanosurf AG, Liestal, Switzerland). Mechanically sharpened Pt/Ir 80/20% wires (Goodfellow Cambridge Limited, Huntingdon, U.K.) are used as tips. Prior to measurements on molecular layers, the bare HOPG substrate is imaged to ensure the quality of the STM tip and the cleanliness of the substrate surface. The tip is then retracted slightly, and a drop of the solution is applied onto the basal plane of HOPG to form a meniscus between the tip and surface. Imaging is thus performed at the solution–solid interface, where typical operating conditions are 1.3 V tunneling voltage and 0.60 nA tunneling current for the molecule and 0.05 V at 1.00 nA for imaging the bare graphite substrate. For imaging graphite through molecules while the surface is covered with solution, the same parameters have been used. A characteristic moiré image is obtained at an intermediate voltage of 0.71 V and 0.68 nA.

## 3. Results and Discussion

Figure 1a shows a typical STM image of the perfectly ordered film exhibiting submolecular resolution. Molecules appear flat-lying and densely packed in rows (lamellae) on the surface, and each molecule appears as two adjacent strands with a total of 19 bright spots representing the protruding hydrogen atoms of the alkyl chains lying parallel to the graphite basal plane.<sup>34</sup> The zigzag arrangement of these spots is the result of a flat orientation of the molecules caused by a series of CH– $\pi$  interactions between the CH group of the alkyl chain and the  $\pi$  electron system of the graphite carbon surface.<sup>35</sup> An enhanced brightness can be observed at the end of each molecule protruding into the interlamellar region that we attribute to hydrogen atoms of the methyl end group. There is an asymmetry within every molecule, with one of the strands appearing brighter than the other, as illustrated by the symbols introduced in Figure 1b. The dark regions between the rows are interpreted as the carboxyl parts of molecules forming dimers which appear darker,<sup>32</sup> an interpretation supported by theoretical modeling.<sup>36,37</sup>

The STM contrast observed in Figure 1a and b allows us to resolve individual molecules and submolecular structures where the periodic brightness modulation is attributed to moiré effects created by the periodic structures of the molecular layer and the substrate surface. It has been reported earlier for carboxylic acids on graphite that there is an apparent periodicity of brightness in the STM image of four or five molecules along the lamellar direction.<sup>21,32,38,39</sup> In our images, an increased brightness appears at every fourth and fifth molecule; however, we note that the true periodicity along the lamella is 10 molecules.

As highlighted in Figure 1b, the molecules marked “0” and “1” flip at every position of enhanced brightness, resulting in an equivalent brightness pattern only at every 10th molecule.

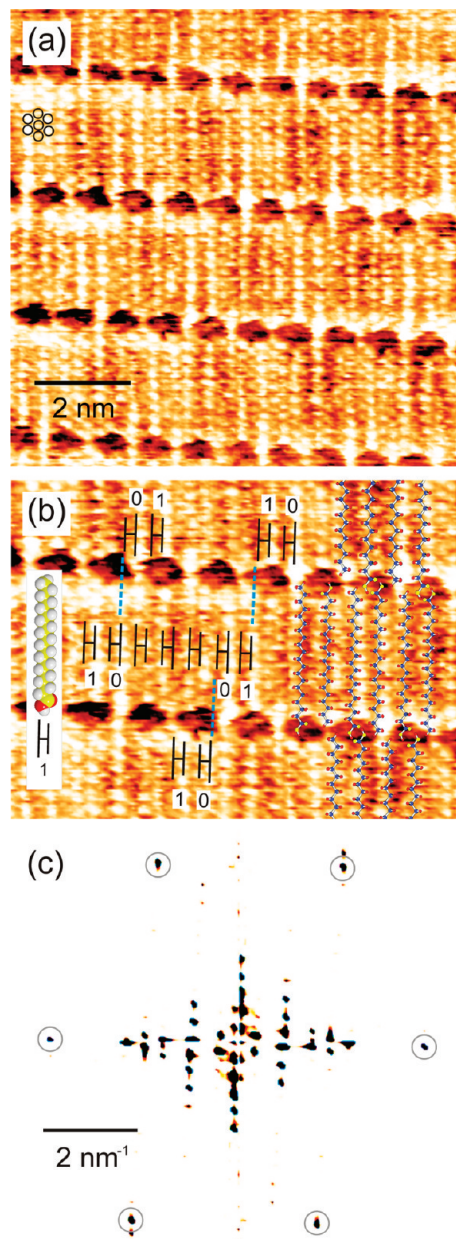


**Figure 1.** (a) High-resolution STM image of an arachidic acid monolayer on HOPG (imaging parameters  $V_b = 1.3$  V and  $I_t = 0.6$  nA). Bright features represent the protruding hydrogen atoms of the all-trans alkyl chains lying parallel in lamellae on the substrate. Dark regions represent carboxyl groups joined by H-bonds. The apparent brightness modulation in the lamellae and further details are explained in the text. The group of circles in the upper left highlights a hexagonal arrangement of alkyl chain hydrogen atoms resulting from the assembly of two neighboring chains. (b) Section from frame a with superimposed prong and skeleton models for the arachidic acid molecule. The longer of the two prongs denotes the side of the molecule terminated by an O–H group. Numbers and dashed lines are explained in the text. (c) Fourier power spectrum of the image from frame a. The spots of the outer hexagon marked by circles originate from the hexagonal arrangement of hydrogen atoms highlighted in frame a.

In addition, the periodicity in brightness shifts by two molecular positions in adjacent rows, indicative of the nature of interlamellar hydrogen bonding present. More precisely, the left strand of the zeroth molecule on the top lamella is in line with the right strand of the zeroth molecule in the bottom lamella (see dashed line in Figure 1b).

Figure 1c is the power spectrum of a Fourier transform of the image from Figure 1a. We analyzed 15 of the predominant

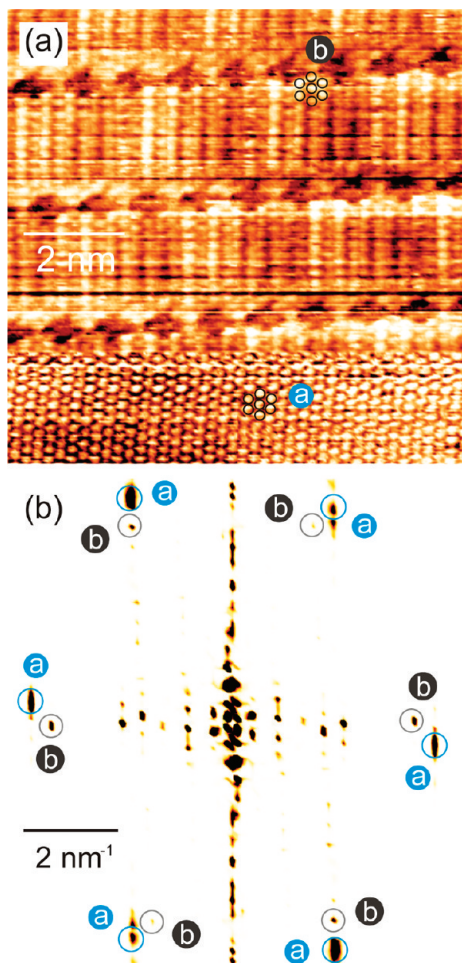


**Figure 2.** (a) Split image showing both the arachidic acid monolayer (upper part,  $V_b = 1.01$  V and  $I_t = 0.73$  nA) and the underlying substrate imaged through the molecules (lower part,  $V_b = 0.05$  V and  $I_t = 1.0$  nA). (b) Fourier power spectrum of the image from frame a. The spectrum reveals two hexagonal lattices, one marked as “a” arising from the graphite and the other one marked as “b” arising from the protruding hydrogen atoms of the adsorbate layer. The apparent distortion of the hexagons is due to thermal drift.

spots in the power spectrum and developed a speculative interpretation for their origin. However, due to the complicated internal structure of the molecular layer and the moiré effects, an unambiguous interpretation of the power spectrum is not possible. Most relevant for our aim to precisely determine the structure, however, we can clearly identify a hexagonal arrangement of spots originating from the protruding hydrogen atoms of the molecules (see hexagon marked by small circles in Figure 1a) that closely but not perfectly resembles the periodic structure of the underlying substrate.

To elucidate this in detail, we take split images obtained by changing the tunneling parameters during imaging, such as the one shown in Figure 2a where both the graphite and the adsorbate monolayer appear in the same frame. In the corresponding Fourier spectrum, one can see two sets of spots with hexagonal symmetry, one arising from the graphite (marked “a”) and the other from the hydrogen atoms of the molecules (marked “b”). The analysis of the Fourier spots of such split images would principally allow a calibration of spots corresponding to the molecular structure against the graphite lattice but is practically difficult due to thermal drift present in the images.

The image shown in Figure 3a is a low drift split image allowing a simple determination of the direction of the molecule

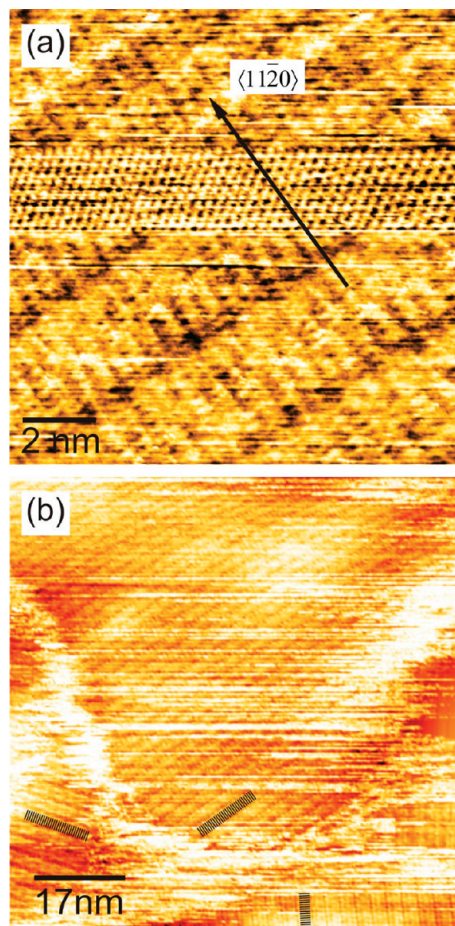


**Figure 3.** (a) High resolution and low drift image similar to the one from Figure 2. The image shows both the molecular layer (top and bottom parts,  $V_b = 1$  V,  $I_t = 0.64$  nA) and the underlying substrate (middle part,  $V_b = 0.05$  V,  $I_t = 1$  nA). The bright spots in the graphite part represent the  $\beta$  carbon atoms of the graphite (0001) surface as imaged by STM. Molecules are found to be aligned along the  $\langle 11\bar{2}0 \rangle$  graphite direction. (b) Large scale image of a molecular layer exhibiting directional domains oriented at  $120^\circ$  relative to each other according to the three equivalent crystallographic directions on the graphite surface. Black lines drawn in stripes schematically represent molecules ordered in lamellae.

with respect to the substrate. The bright spots in the graphite part represent the so-called  $\beta$  carbon atoms of the graphite (0001) crystal plane as imaged by STM.<sup>40</sup> The molecules are found to be aligned along the  $\langle 11\bar{2}0 \rangle$  directions of graphite. Figure 3b is a large frame scan demonstrating that self-assembly occurs in domains oriented  $120^\circ$  relative to each other with molecules following the three equivalent crystallographic directions on the graphite surface. In this image, individual molecules are difficult to resolve, but three rows of molecules are highlighted by black stripes. We observe a blurred contrast hiding molecular details at the domain boundaries and bright stripes in the fast scan direction pointing to irregular tip–molecule interaction at the domain boundaries.

The STM is an ideal tool to study symmetries and chirality at the molecular level.<sup>17,33,41–43</sup> It has been demonstrated that fatty acids with an even number of carbon atoms are pro-chiral and exhibit surface arrangements different from those with an odd number of carbon atoms. The even–odd effect arises from steric hindrance when adsorbed on the surface.<sup>44</sup> Even-numbered molecules exhibit enantiomeric separation, and layers formed of odd-numbered molecules do not exhibit any chirality effect.<sup>31,33,43</sup> Arachidic acid is a pro-chiral molecule due to the

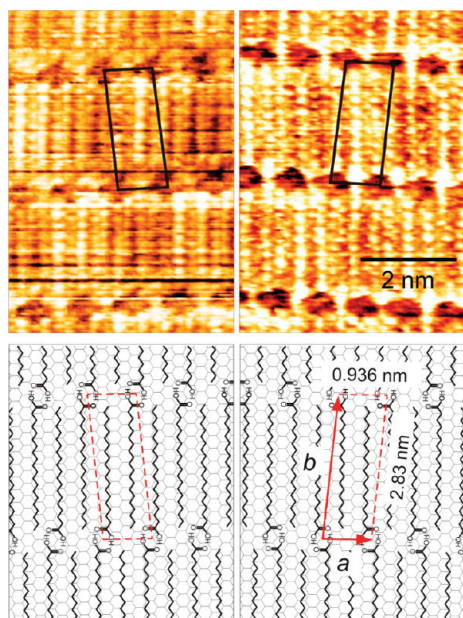


**Figure 4.** STM images demonstrating spontaneous separation of enantiomers observed upon physisorption of arachidic acid on HOPG (imaging parameters for image on the left,  $V_b = 1.01$  V,  $I_t = 0.73$  nA; for the other,  $V_b = 1.3$  V,  $I_t = 0.6$  nA). Although the molecule directions are the same in both images, the oblique unit cells are the mirror images of each other, where the  $\mathbf{b}$  vectors of the unit cells include an angle of  $10^\circ$  with respect to each other. The choice of the unit cell and its dimensions are discussed in the text and also refer to the unit cell shown in Figure 6.

molecular asymmetry introduced by the carboxyl group, and indeed, we find that upon physisorption, arachidic acid molecules tend to arrange in enantiomeric separated domains, as shown in Figure 4. The chirality in the monolayer is evident from the mirror symmetric oblique unit cells that will be discussed in detail below. Here, we note that although the direction of the molecules is the same in both images, the unit cells are mirror images of each other and cannot be superimposed on each other by any 2D translational or rotational symmetry operation. The long sides of the unit cells are tilted by  $\pm 5^\circ$  with respect to the molecular axis, as will be discussed in detail below and, hence, enclose an angle of  $10^\circ$  with respect to each other.

For a precise determination of the intermolecular distance of the structure seen in Figure 1 using an intrinsic calibration with the graphite surface atomic structure as a reference, we use a characteristic moiré image, as shown in Figure 5, that is observed for specific tunneling conditions; namely, a gap voltage between the values for imaging the molecular layer and the graphite substrate, in conjunction with special tip conditions. For the interpretation of the moiré structure caused by the superposition of the monolayer molecular structure and the graphite atomic structure, we recall that simple alkanes adsorb on graphite in registry with the substrate atomic structure;<sup>21</sup> however, for the adsorption of arachidic acid, the steric hindrance imposed by the bulky carboxyl group causes incommensurability along the lamellar direction.

Although the detailed influence of the substrate in the STM image contrast for molecular layers has long been a matter of debate,<sup>36,37,45–50</sup> the resulting contrast can be interpreted straightforwardly. The moiré pattern exhibits a periodicity of  $n_{\text{mol}} = 5$  molecules. From this, the intermolecular distance,  $d_{\text{mol}}$ , can be calculated as  $d_{\text{mol}} = n_{\text{graph}} \times d_{\text{graph}}/n_{\text{mol}}$ , where  $d_{\text{graph}} = 0.213$  nm is the periodicity of the graphite atomic lattice. The number

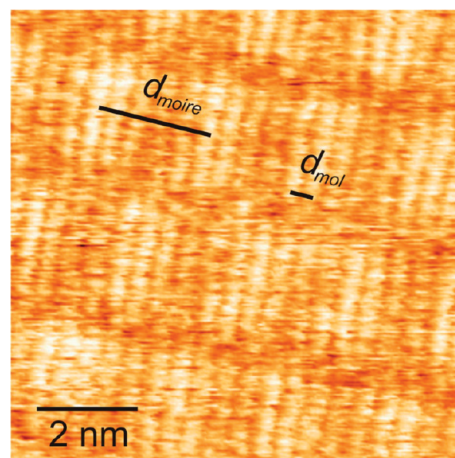


**Figure 5.** Moiré pattern apparent on an arachidic acid monolayer on HOPG exhibiting a periodicity of five molecules (imaging parameters:  $V_b = 0.71$  V and  $I_t = 0.68$  nA). The parameters  $d_{\text{moiré}}$  and  $d_{\text{mol}}$  denote the moiré periodicity distance and the intermolecular distance, respectively.

of graphite periods between molecules that are equivalently positioned with respect to the graphite lattice is assumed to be  $n_{\text{graph}} = 11$ . This is a plausible value because the periodicity would be 10 for simple alkane chains strung along the lamella, and arachidic acid molecules require only little more space due to the carboxylic end group. From this analysis, we obtain a value for the intermolecular distance of  $d_{\text{mol}} = 0.486$  nm and can adjust earlier propositions of a larger intermolecular distance that were based on a wrong assumption for the brightness modulation periodicity.<sup>32</sup>

In Figure 6, we present the proposed model for the molecular assembly in the form of lamellae joined by pairs of carboxyl groups. As will be discussed in detail below, this model is chosen from three different models as the one that fits best to the experimentally observed unit cell dimensions facilitating hydrogen bonding between the carboxylic end groups in addition to the van der Waals interactions between the hydrocarbon chains.

To identify the true molecular assembly model, we construct three models that are all based on the intermolecular distance of 0.47 nm as it has been determined in the previous section. We assume that molecules attain the optimum adsorption position for those molecules marked “1” and are close to the optimum for molecules marked “0”. Intermediate positions along the lamella are less energetically favorable. However, (close to) optimum adsorption conditions are found for every fourth and fifth molecule. This explains the experimentally observed modulation in STM contrast as highlighted in Figure 1b, assuming that the tunnel current is influenced by the relative position of the H atoms of the molecules and the carbon atoms of the substrate.

To visualize this for the optimum model, in Figure 6, we combine a hexagonal network of graphite  $\beta$  carbon atoms with the molecular model. Note that the bright blobs seen in the STM image correspond to the hydrogen atoms and not the carbon backbone.<sup>34</sup> The three different models are the result of allowing the molecules to occupy only those graphite lattice sites along the molecular axis that can produce the observed STM contrast modulation, and that are compatible with attaining an optimum adsorption position for every fifth molecule. Because the modulation is related to the electronic interaction between the molecular layer and the graphite substrate, we move one of the molecular rows by equal steps of the graphite zigzag distance

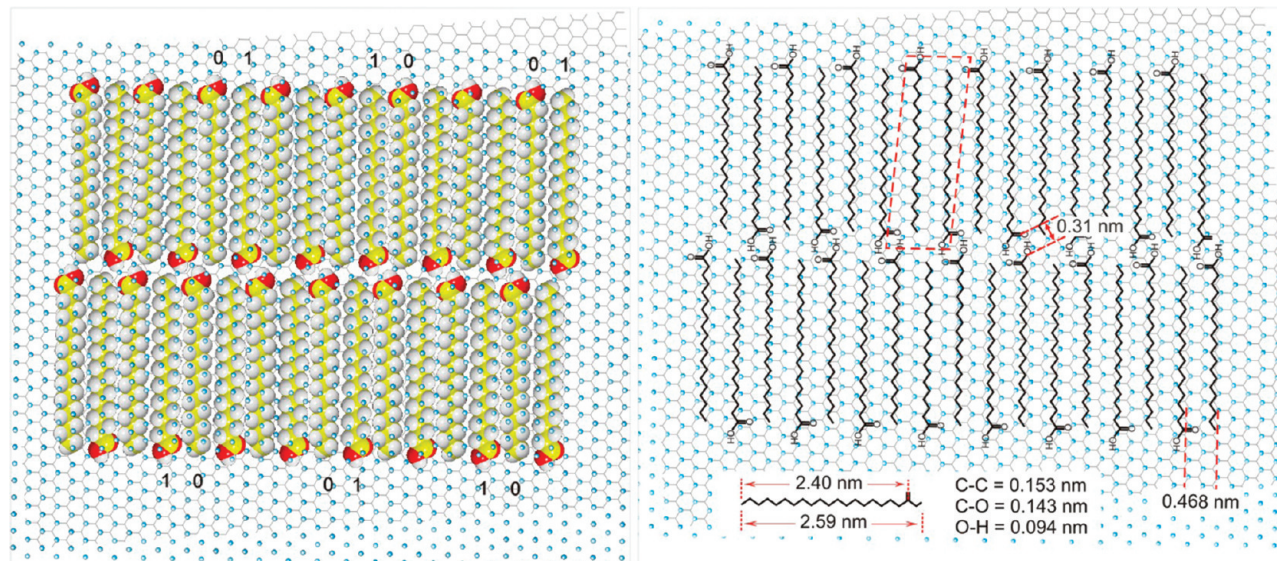


**Figure 6.** Space-fill and skeleton models for the molecular arrangement of arachidic acid on HOPG (model b in Table 1) superimposed with the hexagonal grid of  $\beta$  carbon atoms of the graphite surface. Bond lengths in the hydrocarbon skeletal chains are drawn to scale. The length of the molecule is determined by a construction based on known bond lengths and bond angles taken from literature.<sup>45,46,51,52</sup>

**TABLE 1: Unit Cell and H-Bonding Parameters for Possible Models of the Arachidic Acid Self-Assembled Monolayer on HOPG**

model	unit cell dimensions (nm), angle between unit cell vectors	O—O distance (nm) derived from structure model
a	$a = 0.936$ $b = 2.95$ $85^\circ$	0.44
b	$a = 0.936$ $b = 2.83$ $85^\circ$	0.31
c	$a = 0.936$ $b = 2.71$ $85^\circ$	0.20

of 0.123 nm, resulting in the three models a, b, and c with unit cell parameters described in Table 1. The true unit cell dimension,  $|b|$ , is obtained by an analysis of the respective dimension in the models and the known length of the arachidic acid molecule. The length of the arachidic acid molecule can be calculated to be 2.40 nm from the terminating carbon to the C=O bond, as shown in Figure 6 from the known lengths and angles of the involved bonds.<sup>45,46,51,52</sup> Using this value and relating the molecular length to the unit cell dimension  $|b|$  in the model drawn in Figure 6 precisely reproduces the prediction from model b that is  $|b| = 2.83$  nm.

The choice of model b as the true molecular assembly structure is further supported by considering the carboxyl–carboxyl interlamellar hydrogen bonding. It is known that carboxylic acids can form dimers in media of low dielectric constant. However, we are not aware of a report on the accurate O—O distance for a carboxylic dimer on graphite. This leaves some uncertainty when constructing molecular arrangement models like, for example, the one reported for cis-unsaturated carboxylic acids.<sup>31</sup> Long before the advent of scanning probe techniques, it was suggested, however, purely from geometric considerations that the O—O distance for the carboxylic cyclic dimer on graphite could take a value less than 0.20 nm or greater than 0.35 nm, provided both molecules on adjacent lamellae are in a “lattice fit” arrangement (as for alkanes<sup>53</sup>) and 0.28 nm when only one of them occupies the “lattice fit” arrangement.<sup>52</sup>

But when molecules are embedded on graphite like in a monolayer, there can be sites where molecules in adjacent lamellae forming a dimer are possibly out of any “lattice fit” arrangement. Another issue is that here, measurements are performed in a liquid environment, and in general, the polarity of the solvent can affect the hydrogen bond strength due to the electrostatic and charge-transferring nature of the hydrogen bond.<sup>54</sup> Because phenyloctane is a nonpolar solvent, this effect can probably be neglected here.

Practically, the O—O distance can be obtained only after a suitable model is constructed and the molecular positions are precisely fixed as for the model shown in Figure 1b. For our purpose, we compare values derived from the models to the gas phase value of the O—O distance. Both theoretical<sup>55</sup> and experimental<sup>56</sup> gas phase values for the enthalpy of carboxyl dimerization have been determined to be  $-60$  kJ mol<sup>-1</sup>, and the O—O distance for optimum binding has been found to be 0.28 nm.<sup>55</sup> Also in light of these considerations, we conclude that model b assuming an O—O bond distance of 0.31 nm is the energetically most favorable one because this value is closest to the gas phase value. Note that this is an unrelaxed value resulting from purely geometric considerations. The actual O—O bond distance might be slightly different due to molecular relaxation, possibly yielding an energetically more favorable configuration.

At this point, we can define all dimensions of the oblique unit cell of the molecular structure from model b as  $|a| = 0.94$  nm and  $|b| = 2.83$  nm where the angle between unit cell vectors **a** and **b** is  $85^\circ$ . The unit cell accommodates two molecules and is tilted by  $5^\circ$  with respect to the molecular axis. Note, that this is the unit cell of the molecular structure but not the unit cell of the STM image that is influenced by moiré effects. A close inspection of the STM image reveals variations in apparent contrast between nominally equivalent molecules that imply a much larger unit cell than determined above. This is also reflected in the Fourier spectra from Figures 1 and 2, where the dimensions of the structural unit cell are not clearly represented as dominating spots. The relation between the structural and the STM image unit cell is determined by details of the superposition of tunnel current contributions from the molecular

layer and the substrate and remains to be determined in detail by a STM image calculation.

#### 4. Conclusion

Arachidic acid forms well-ordered monolayers by molecular self-assembly with molecules lying flat on the surface in rows that are stabilized via side-by-side van der Waals interactions between the aliphatic chains. Stabilization between rows is facilitated by hydrogen double-bonds formed pairwise between carboxyl groups of molecules from neighboring rows. We observe domains with rows oriented in three different directions compatible with the 3-fold symmetry of the graphite surface. Because arachidic acid is a pro-chiral molecule, we observe enantiomeric separation into molecular domains having unit cells that are tilted by 10° with respect to each other. The deviation of registry between alkyl chains and the graphite lattice results in peculiar contrast features in STM imaging in the form of an asymmetric appearance of the molecules, periodic contrast enhancement, and a characteristic moiré pattern observed under certain experimental conditions. Using methods of internal calibration of the STM images with respect to the graphite surface atomic structure, we unambiguously determine the oblique monolayer unit cell (85° angle) with dimensions of 0.94 nm × 2.83 nm, allowing for a favorable, unrelaxed O—O distance of 0.31 nm for hydrogen bonding between carboxylic dimers.

**Acknowledgment.** This work has been supported by the Ph.D. program “Synthesis and Characterization of surfaces and Interfaces assembled from Clusters and Molecules” and by the Deutsche Forschungsgemeinschaft (DFG) through the Emmy Noether-Programm.

#### References and Notes

- (1) Forrest, S. R. *Nature* **2004**, *428*, 911–918.
- (2) De Feyter, S.; Uji-i, H.; Mamdouh, W.; Miura, A.; Zhang, J.; Jonkheijm, P.; Schenning, A.; Meijer, E. W.; Chen, Z.; Wurthner, F.; Schuurmans, N.; van Esch, J.; Feringa, B. L.; Dulcey, A. E.; Percec, V.; De Schryver, F. C. *Int. J. Nanotechnol.* **2006**, *3*, 462–479.
- (3) Joachim, C.; Gimzewski, J. K.; Aviram, A. *Nature* **2000**, *408*, 541–548.
- (4) Shaw, J. M.; Seidler, P. F. *IBM J. Res. Dev.* **2001**, *45*, 3–9.
- (5) Grätzel, M. *Nature* **2001**, *414*, 338–344.
- (6) Barlow, S. M.; Raval, R. *Surf. Sci. Rep.* **2003**, *50*, 201–341.
- (7) Rosei, F.; Schunack, M.; Naitoh, Y.; Jiang, P.; Gourdon, A.; Lægsgaard, E.; Stensgaard, I.; Joachim, C.; Besenbacher, F. *Prog. Surf. Sci.* **2003**, *71*, 95–146.
- (8) Barth, J. V.; Costantini, G.; Kern, K. *Nature* **2005**, *437*, 671–679.
- (9) Otero, R.; Rosei, F.; Besenbacher, F. *Annu. Rev. Phys. Chem.* **2006**, *57*, 497–525.
- (10) Barth, J. V. *Annu. Rev. Phys. Chem.* **2007**, *58*, 375–407.
- (11) Kühnle, A. *Curr. Opin. Colloid Interface Sci.* **2009**, *14*, 157–168.
- (12) Linares, M.; Minoia, A.; Brocorens, P.; Beljonne, D.; Lazzaroni, R. *Chem. Soc. Rev.* **2009**, *38*, 806–816.
- (13) Bombis, C.; Weigelt, S.; Knudsen, M. M.; Norgaard, M.; Busse, C.; Lægsgaard, E.; Besenbacher, F.; Gothelf, K. V.; Linderth, T. R. *ACS Nano* **2010**, *4*, 297–311.
- (14) Smith, W. F. *Nat. Nanotechnol.* **2007**, *2*, 77–78.
- (15) Schenning, A.; Meijer, E. W. *Chem. Commun.* **2005**, 3245–3258.
- (16) Mendes, P. M.; Flood, A. H.; Stoddart, J. F. *Appl. Phys. A: Mater. Sci. Process.* **2005**, *80*, 1197–1209.
- (17) De Feyter, S.; De Schryver, F. C. *Chem. Soc. Rev.* **2003**, *32*, 139–150.
- (18) De Feyter, S.; De Schryver, F. C. *J. Phys. Chem. B* **2005**, *109*, 4290–4302.
- (19) Amabilino, D. B.; De Feyter, S.; Lazzaroni, R.; Gomar-Nadal, E.; Veciana, J.; Rovira, C.; Abdel-Mottaleb, M. M.; Mamdouh, W.; Iavicoli, P.; Psychogioyopoulou, K.; Linares, M.; Minoia, A.; Xu, H.; Puigmarti-Luis, J. *J. Phys.: Condens. Matter* **2008**, *20*, 184003.
- (20) Foster, J. S.; Frommer, J. E. *Nature* **1988**, *333*, 542–545.
- (21) Rabe, J. P.; Buchholz, S. *Science* **1991**, *253*, 424–427.
- (22) Cincotti, S.; Rabe, J. P. *Appl. Phys. Lett.* **1993**, *62*, 3531–3533.
- (23) McGonigal, G. C.; Bernhardt, R. H.; Thomson, D. J. *Appl. Phys. Lett.* **1990**, *57*, 28–30.
- (24) Rabe, J. P.; Buchholz, S. *Phys. Rev. Lett.* **1991**, *66*, 2096–2099.
- (25) Couto, M. S.; Liu, X. Y.; Meekes, H.; Bennema, P. *J. Appl. Phys.* **1994**, *75*, 627–629.
- (26) Venkataraman, B.; Breen, J. J.; Flynn, G. W. *J. Phys. Chem.* **1995**, *99*, 6608–6619.
- (27) Venkataraman, B.; Flynn, G. W.; Wilbur, J. L.; Folkers, J. P.; Whitesides, G. M. *J. Phys. Chem.* **1995**, *99*, 8684–8689.
- (28) Magonov, S. N.; Wawkuszewski, A.; Cantow, H. J.; Liang, W.; Whangbo, M. H. *Appl. Phys. A: Mater. Sci. Process.* **1994**, *59*, 119–133.
- (29) Cyr, D. M.; Venkataraman, B.; Flynn, G. W. *Chem. Mater.* **1996**, *8*, 1600–1615.
- (30) De Feyter, S.; Gesquière, A.; Abdel-Mottaleb, M. M.; Grim, P. C. M.; De Schryver, F. C.; Meiners, C.; Sieffert, M.; Valiyaveetil, S.; Müllen, K. *Acc. Chem. Res.* **2000**, *33*, 520–531.
- (31) Tao, F.; Goswami, J.; Bernasek, S. L. *J. Phys. Chem. B* **2006**, *110*, 4199–4206.
- (32) Hibino, M.; Sumi, A.; Hatta, I. *Jpn. J. Appl. Phys.* **1995**, *34*, 610–614.
- (33) Hibino, M.; Sumi, A.; Tsuchiya, H.; Hatta, I. *J. Phys. Chem. B* **1998**, *102*, 4544–4547.
- (34) Liang, W.; Whangbo, M. H.; Wawkuszewski, A.; Cantow, H. J.; Magonov, S. N. *Adv. Mater.* **1993**, *5*, 817–821.
- (35) Perez-Garcia, L.; Amabilino, D. B. *Chem. Soc. Rev.* **2002**, *31*, 342–356.
- (36) Faglioni, F.; Claypool, C. L.; Lewis, N. S.; Goddard, W. A. *J. Phys. Chem. B* **1997**, *101*, 5996–6020.
- (37) Yang, T.; Berber, S.; Liu, J. F.; Miller, G. P.; Tomanek, D. *J. Chem. Phys.* **2008**, *128*, 124709.
- (38) Hibino, M.; Sumi, A.; Hatta, I. *Jpn. J. Appl. Phys.* **1995**, *34*, 3354–3359.
- (39) Hibino, M.; Sumi, A.; Hatta, I. *Thin Solid Films* **1996**, *273*, 272–278.
- (40) Tomanek, D.; Louie, S. G.; Mamin, H. J.; Abraham, D. W.; Thomson, R. E.; Ganz, E.; Clarke, J. *Phys. Rev. B* **1987**, *35*, 7790–7793.
- (41) Fang, H. B.; Giancarlo, L. C.; Flynn, G. W. *J. Phys. Chem. B* **1998**, *102*, 7421–7424.
- (42) Kühnle, A.; Linderth, T. R.; Hammer, B.; Besenbacher, F. *Nature* **2002**, *415*, 891–893.
- (43) Tao, F.; Bernasek, S. L. *J. Phys. Chem. B* **2005**, *109*, 6233–6238.
- (44) Nath, K. G.; Ivasenko, O.; MacLeod, J. M.; Miwa, J. A.; Wuest, J. D.; Nanci, A.; Perepichka, D. F.; Rosei, F. *J. Phys. Chem. C* **2007**, *111*, 16996–17007.
- (45) Hentschke, R.; Schurmann, B. L.; Rabe, J. P. *J. Chem. Phys.* **1992**, *96*, 6213–6221.
- (46) Hentschke, R.; Winkler, R. G. *J. Chem. Phys.* **1993**, *99*, 5528–5534.
- (47) Richter, S.; Manassen, Y. *J. Phys. Chem.* **1994**, *98*, 2941–2949.
- (48) Claypool, C. L.; Faglioni, F.; Goddard, W. A.; Gray, H. B.; Lewis, N. S.; Marcus, R. A. *J. Phys. Chem. B* **1997**, *101*, 5978–5995.
- (49) Lazzaroni, R.; Calderone, A.; Bredas, J. L.; Rabe, J. P. *J. Chem. Phys.* **1997**, *107*, 99–105.
- (50) Ilan, B.; Florio, G. M.; Hybertsen, M. S.; Berne, B. J.; Flynn, G. W. *Nano Lett.* **2008**, *8*, 3160–3165.
- (51) Lide, D. R.; Frederikse, H. P. R. *CRC Handbook of Chemistry and Physics*, 83th ed.; CRC Press: Boca Raton, 2003.
- (52) Findenag, J. *Chem. Soc., Faraday Trans. 1* **1973**, *69*, 1069–1078.
- (53) Groszek, A. *J. Proc. R. Soc. London A* **1970**, *314*, 473–498.
- (54) Aquino, A. J. A.; Tunega, D.; Haberhauer, G.; Gerzabek, M. H.; Lischka, H. *J. Phys. Chem. A* **2002**, *106*, 1862–1871.
- (55) Bures, M.; Bezus, J. *Collect. Czech. Chem. Commun.* **1994**, *59*, 1251–1269.
- (56) Chocholousova, J.; Vacek, J.; Hobza, P. *J. Phys. Chem. A* **2003**, *107*, 3086–3092.